

# Low-temperature biaxial nematic from rod and disc mesogen mixture

Roberto Berardi<sup>\*a</sup> and Claudio Zannoni<sup>a</sup>

Received Xth XXXXXXXXXXXX 20XX, Accepted Xth XXXXXXXXXXXX 20XX

First published on the web Xth XXXXXXXXXXXX 200X

DOI: 10.1039/b000000x

Molecular dynamics computer simulations have been employed to demonstrate that the addition of a suitable uniaxial discotic nematic to a biaxial nematic ( $N_b$ ) of elongated mesogens can give rise to a low temperature  $N_b$  liquid crystal (where the rod-like particles would form a biaxial smectic). The two species are made to be fully miscible over the entire isotropic and nematic temperature range by a suitable parameterisation of shapes and pair interactions. The disc-like mesogen, even though not forming a biaxial nematic by itself gives a stable low-temperature discotic nematic which strongly disfavours the formation of columnar and smectic phases in the two-components system.

## 1 Introduction

The development of biaxial nematics ( $N_b$ ) promises to open up a new generation of displays and other electro-optic devices, through the control of the orientation of two, rather than one, directors *i.e.*, the preferred directions of alignment of the liquid crystalline material<sup>1</sup>.

Although the first  $N_b$ s discovered, and the only ones for a long time, have been lyotropics<sup>2,3</sup>, polymeric<sup>4</sup>, or, more recently, polydisperse mixtures of board-like goethite particles<sup>5,6</sup>, hardly suitable for normal displays, in the last few years relatively low molar mass thermotropics have been reported for various classes of molecules ranging from bent-core<sup>7,8</sup> or V-shaped<sup>9</sup>, to flexible silicon tetrapodes<sup>10</sup>.

Besides these successes, none of the currently available thermotropic  $N_b$  materials still appear to be easily utilisable in practical electro-optic devices either because of their very high temperature nematic range (*e.g.* over 373 K for the bent-core mesogens in refs.<sup>7,8</sup>), or because of their high viscosity<sup>11</sup> and slow response. Therefore,  $N_b$  mesogens are still actively pursued, and even if tuning the properties of materials, and liquid crystals in particular, is an art that synthetic chemists have perfected (see *e.g.* for reviews<sup>1,12,13</sup>). The difficulty here lies in obtaining a  $N_b$ , rather than one of the competing phases, such as a uniaxial nematic, biaxial smectic or crystalline solid, when attempting molecular modifications around the known mesogenic molecular structures. The risk seems to be particularly high for the

**Table 1** Parameters of the biaxial GB potential for the model mesogens used in this work. Ellipsoids axes  $\sigma_a^{(i)}$  are in  $\sigma_0$  units, well depths  $\epsilon_a^{(i)}$  are in  $\epsilon_0$  units, while masses  $m_i$  are in  $m_0$  units. The exponents  $\mu = 1$ ,  $\nu = 3$ , and the parameter  $\sigma_c = 0.714 \sigma_0$ . The dimensionless scaling parameters used for the homogeneous rod-rod and disc-disc interactions were  $e_{rod-rod} = e_{disc-disc} = 1$ , while for the heterogeneous rod-disc ones we used  $e_{rod-disc} = 1.8$

type $i$	$m_i$	$\sigma_x^{(i)}$	$\sigma_y^{(i)}$	$\sigma_z^{(i)}$	$\epsilon_x^{(i)}$	$\epsilon_y^{(i)}$	$\epsilon_z^{(i)}$
rod	3	1.4	0.714	3	1	0.9	0.2
disc	2	1.4	2	0.714	1.29	1.6	0.2

important task of lowering the biaxial nematic transition temperature while avoiding the formation of smectics as, for instance, favouring *face-to-face* packing will help in making the organisation biaxial, but not necessarily nematic<sup>14</sup>. As an alternative to obtaining a suitable one-component mesogenic material, another chemical way of tuning properties is that of employing mixtures, and indeed many of the commercial products actually offered by industry in liquid crystal displays are uniaxial formulations of various (up to 5–7) components.

Binary mixtures of uniaxial elongated (rod-like) and squashed (disc-like) mesogens have been recognised by Alben more than thirty years ago<sup>15</sup> as a possible pathway towards a thermotropic  $N_b$ . The rationale is particularly simple and appealing: whenever packing density increases the uniaxial rods and discs will align in the nematic phase along two mutually orthogonal directions and, as long as the two species are miscible, a macroscopic

<sup>a</sup> Dipartimento di Chimica Fisica e Inorganica, Università di Bologna, Bologna, Italy, Fax: +39 051 2093690; Tel: +39 051 2093387; E-mail: Roberto Berardi (roberto.berardi@unibo.it)

ically  $N_b$  phase should result<sup>15,16</sup>.

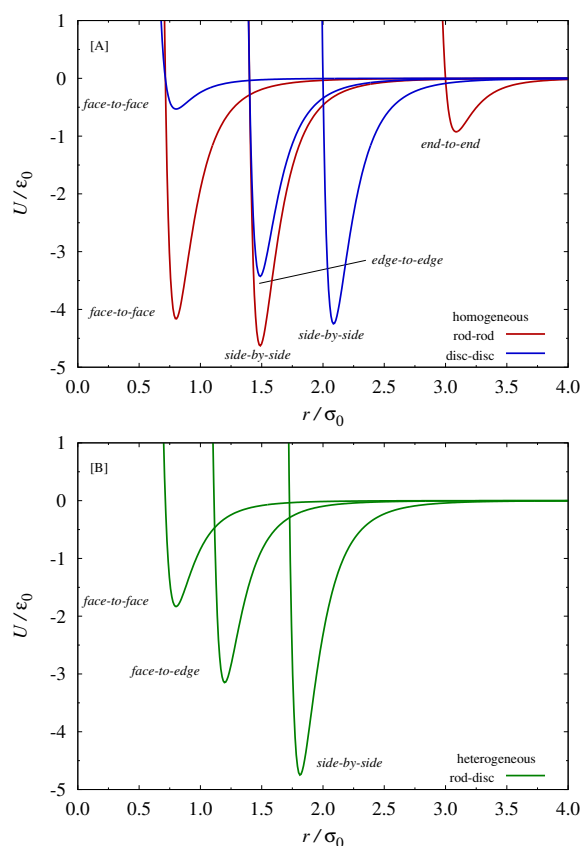


**Fig. 1** Representative Gay–Berne energy profiles for the homogeneous (plate A) rod–rod (solid, red) and disc–disc (dashed, blue), and heterogeneous (plate B) rod–disc (dotted, green) pair interactions in the *side-by-side*, *face-to-face*, and *end-to-end* configurations using the parameterisation described in the text and Table 1

Unfortunately, Alben’s sketch assumes as a necessary prerequisite the full miscibility of the molecular species over the entire phase diagram (or at least over the range of temperatures used in the target applications). This assumption severely limits the possibilities offered by mixing. Indeed, full mixing is expected for mesophases of the same nature and this is often a technique used to assign a phase to one of the known types<sup>17,18</sup>. However, the formation of a homogeneous phase can not be taken for granted when using molecules of different shapes resulting from very different chemical structures, like elongated and squashed thermotropic mesogens. As it comes out, the general outcome of most experiments<sup>19–21</sup>, as well as theories<sup>22–29</sup>, and computer simulations<sup>30</sup> is that rod-like and disc-like mesogens (either with typical molecular shapes or approximating the infinitely long or thin

limit) will eventually demix at low-temperatures and/or high-density.

Several strategies have been attempted to avoid demixing, connecting rod-like and disc-like mesogens by weak bonds<sup>31</sup> or flexible linkers<sup>32</sup>. Experiments relying on enhanced lateral interactions<sup>33,34</sup> or shape amphiphiles<sup>35,36</sup>, have not been successful so far<sup>13</sup>, unless in the presence of an external electric field<sup>37</sup>. The situation has recently started changing for the better. In particular, Kouwer and Mehl<sup>38</sup>, and Apreutesei and Mehl<sup>39</sup> have experimentally demonstrated the full miscibility of certain rod-like and disc-like mesogens, and even though these mixtures are not  $N_b$  themselves, this result demonstrates that the entropic-driven demixing process can be surmounted. Bates, Vanakaras and Photinos<sup>40</sup> have shown by Monte Carlo (MC) computer simulations how by properly choosing the shapes of hard biaxial brick-like particles this entropic hindrance can be overcome at least when the long axes are completely ordered. Furthermore, avoiding the strong limitation of complete order Jackson and coworkers<sup>41</sup> have shown, also by MC simulations, that  $N_b$  phases can be obtained by mixing elongated spherocylinders and discotic cut-spheres with suitably tailored anisotropic heterogeneous attractions between the otherwise hard particles. On the experimental side the findings of Vroege and co-workers<sup>5,6</sup>, even though involving colloidal mixtures of polydisperse biaxial clay platelets (and not single molecule systems), have demonstrated how the shape polydispersity of colloidal particles favours  $N_b$  phases by inhibiting the formation of highly ordered and densely packed smectic or solid organisations. The theoretical model of Ratón and Cuesta<sup>42</sup> gives an interpretation of this behaviour and predicts stable biaxial nematics from polydispersed mixtures of elongated and squashed uniaxial hard parallelepipeds.

In this paper, we wish to show that even using just a monodisperse binary mixture we can, by tuning both shape and molecular interactions, effectively counteract demixing and realise a low temperature  $N_b$  phase. In particular, we believe this can be done by mixing elongated and squashed biaxial mesogenic particles interacting via an anisotropic attractive–repulsive anisotropic potential which does not involve specific weakly bonding rod–disc interactions but which confers a dual calamitic–discotic mesogenic nature to both molecular species. To demonstrate it we have deployed molecular dynamics (MD) simulations of elongated and squashed attractive–repulsive biaxial ellipsoids.

The plan of the manuscript is as follows: in Section 2 we show the pair potential and the parameterisation used for the mesogenic particles; in Section 3 we report the technical details of the computer simulations; in Section 4

we discuss the MD results; eventually some final remarks conclude the paper. In the Appendix we describe the algorithm devised for the computation of global order parameters for a two-components mixture of biaxial ellipsoids.

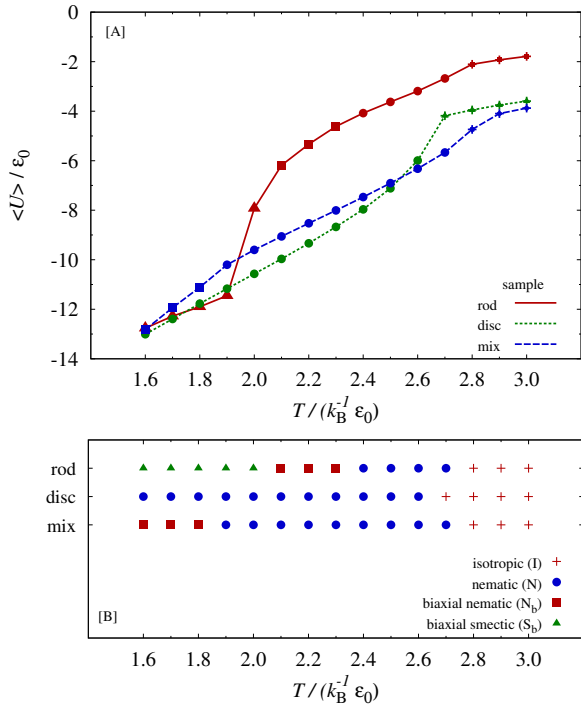


**Fig. 2** Average dimensionless potential energy per particle  $\langle U^* \rangle = \langle U \rangle / \epsilon_0$  (plate A), and sequence of phases (plate B) as a function of dimensionless temperature from a cooling-down sequence of MD simulations of the three  $N = 4096$  systems described in the text. The phases observed are identified as biaxial smectic  $S_b$  (filled triangles), biaxial nematic  $N_b$  (filled squares), uniaxial nematic  $N$  (filled circles), and isotropic (I) (crosses). Error bars in plate A (see also Tables 1, 2, and 3) are typically smaller than the symbol size and are not appreciable in this representation

## 2 Molecular model

The anisotropic pair interaction between the mesogenic species of this work has been computed by the biaxial extension of the Gay–Berne (GB) potential<sup>43–45</sup> between two rigid ellipsoidal particles of species  $\alpha$  and  $\beta$  (see also<sup>46</sup> for another formulation). The GB energy is parameterised in terms of the ellipsoids axes lengths  $\sigma_x^{(i)}$ ,  $\sigma_y^{(i)}$ ,  $\sigma_z^{(i)}$ , and of the interaction strengths  $\epsilon_x^{(i)}$ ,  $\epsilon_y^{(i)}$  and  $\epsilon_z^{(i)}$ , with  $i = \alpha$ , or  $\beta$ . The coefficients  $\epsilon_x^{(i)}$  are proportional to the well depths for the *side-by-side*, *face-to-face*, and *end-to-end* interactions<sup>45</sup>. Two exponents  $\mu$ ,  $\nu$

and the minimum contact distance  $\sigma_c$  allow to tune the shape of the energy wells<sup>44,45,47</sup>. The potential between a pair 1, 2 of biaxial molecules of species  $\alpha$  and  $\beta$  can be written as

$$U(\mathbf{r}, \mathbf{Q}) = 4\epsilon_0 \epsilon(\mathbf{r}, \mathbf{Q}) [u^{12}(\mathbf{r}, \mathbf{Q}) - u^6(\mathbf{r}, \mathbf{Q})], \quad (1)$$

where  $u(\mathbf{r}, \mathbf{Q}) = \sigma_c / (r - \sigma(\mathbf{r}, \mathbf{Q}) + \sigma_c)$ . The distance and energy units are  $\sigma_0$  and  $\epsilon_0$ . The symbol  $\mathbf{Q}$  stands here for the two quaternions<sup>48,49</sup>  $[\mathbf{q}^{(1)}]$ , and  $[\mathbf{q}^{(2)}]$  defining the orientations of the two particles in the laboratory frame, while  $\mathbf{r} = \mathbf{r}_2 - \mathbf{r}_1$  is the intermolecular vector, with length  $r$ . The anisotropic contact term is

$$\sigma(\mathbf{r}, \mathbf{Q}) = r [2\mathbf{r}^T \mathbf{A}^{-1} \mathbf{r}]^{-1/2}. \quad (2)$$

The symmetric overlap matrix  $\mathbf{A} \equiv \mathbf{A}(\mathbf{Q})$  is defined in terms of the diagonal “*shape*” matrices  $\mathbf{S}^{(i)}$  as

$$\mathbf{A} = \mathbf{M}^{(1)T} \mathbf{S}^{(\alpha)2} \mathbf{M}^{(1)} + \mathbf{M}^{(2)T} \mathbf{S}^{(\beta)2} \mathbf{M}^{(2)}, \quad (3)$$

where the elements are  $S^{(i)}_{a,b} = \delta_{a,b} \sigma_a^{(i)}$ . The cartesian rotation matrices for the two molecules  $\mathbf{M}^{(n)} \equiv \mathbf{M}(m_n \leftarrow l)$ , with  $n = 1$ , and 2 perform the active rotation from laboratory to molecular frame, and are defined<sup>48,49</sup> in terms of the quaternions  $[\mathbf{q}^{(i)}]$ . The anisotropic interaction term is

$$\epsilon(\mathbf{r}, \mathbf{Q}) = e_{\alpha\beta} \epsilon_A^\nu(\mathbf{Q}) \epsilon_B^\mu(\mathbf{r}, \mathbf{Q}), \quad (4)$$

where the coupling parameter  $e_{\alpha\beta}$  allows to modulate the range of energy surfaces for the interaction of like ( $\alpha = \beta$ ) or unlike ( $\alpha \neq \beta$ ) ellipsoids. The dimensionless strength coefficient  $\epsilon_A$  is

$$\epsilon_A(\mathbf{Q}) = [\sigma_x \sigma_y + \sigma_z^2] \left[ \frac{2\sigma_x \sigma_y}{\det[\mathbf{A}]} \right]^{1/2}, \quad (5)$$

and the dimensionless interaction parameter  $\epsilon_B$  is

$$\epsilon_B(\mathbf{r}, \mathbf{Q}) = 2r^{-2} \mathbf{r}^T \mathbf{B}^{-1} \mathbf{r}. \quad (6)$$

The interaction matrix  $\mathbf{B} \equiv \mathbf{B}(\mathbf{Q})$  is defined in terms of the auxiliary diagonal “*interaction*” matrices  $\mathbf{E}^{(i)}$  as

$$\mathbf{B} = \mathbf{M}^{(1)T} \mathbf{E}^{(\alpha)} \mathbf{M}^{(1)} + \mathbf{M}^{(2)T} \mathbf{E}^{(\beta)} \mathbf{M}^{(2)}, \quad (7)$$

where the elements are  $E^{(i)}_{a,b} = \delta_{a,b} (\epsilon_0 / \epsilon_a^{(i)})^{1/\mu}$ . Explicit expressions for the gradient and torques of the biaxial GB potential are given in refs.<sup>49,50</sup>

The specific parameterisation for the two species of biaxial GB particles with dual behaviour used in this work has been chosen relying on a number of previous results: (a) particles with similar cross section but incommensurate lengths<sup>40</sup>; (b) weakened homogeneous rod–rod and

disc–disc interactions (akin in a sense to weakly attractive rod–disc interactions<sup>31,41</sup>); and (c) opposite shape and interaction biaxialities<sup>47</sup>. All of these properties contribute to achieve several modelling goals: (a) limit the formation of positionally ordered low–temperature organisations; (b) enhance lateral *side-by-side* attractions with respect to *face-to-face* (see Figure 1, and Table 1) to obtain duality; and (c) prevent the demixing between rods and discs (usually taking place at the isotropic–nematic phase transition or at low temperatures). In practice, point (a) has been achieved by means of modelling the shape, as suggested by Vanakaras, Bates and Photinos<sup>40</sup>, so that both prolate and oblate ellipsoids share two axes lengths while the third ones have incommensurate lengths. Regarding points (b) and (c), the  $\epsilon_a^{(i)}$  coefficients for both species (see Table 1), and the parameter  $e_{\text{rod-disc}} = 1.8$ , were chosen to give homogeneous rod–rod and disc–disc and heterogeneous rod–disc interactions of comparable strength (see Figure 1). Regarding the interaction anisotropy, all lateral *side-by-side* attractions were enhanced with respect to those *face-to-face* (especially for disc–disc pairs). Concurrently, the potential surface for rod–rod interactions has a  $\approx 40\%$  weaker *side-by-side* attraction between particles previously studied<sup>47</sup>, to also match the energies between squashed ellipsoids. This tuning of a common attractive–repulsive model is different from the approach of Cuetos, Galindo and Jackson<sup>41</sup> relying on specific rod–disc attractions of a different nature from the purely repulsive homogeneous interactions between hard particles.

With this three–parts recipe both elongated and squashed particles possess a dual nature consisting in steric contribution arising from the shape anisotropy which competes with an opposing enthalpic one due to the attractive part of the potential.

### 3 Systems studied and simulation details

We have performed three series of isobaric–isothermal molecular dynamics simulations on a set of bulk samples formed by  $N = 4096$  biaxial GB particles: two for each one–component systems of elongated and squashed mesogens, and one for their equimolar mixture (see Table 1). The cutoff radius for the GB interactions was  $r_c = 4 \sigma_0$ , and a neighbour list of radius  $r_l = 5 \sigma_0$  was also employed for all simulations. The dimensionless time step was chosen as  $\Delta t^* = (\epsilon_0/\sigma_0^2 m_0)^{1/2} \Delta t = 0.002$ , where  $m_0$  is the unit for mass. The standard velocity–Verlet integrator<sup>51,52</sup> has been used for the translational equations of motions, while the rotational trajectories have been determined using the approach of refs.<sup>49,53,54</sup>.

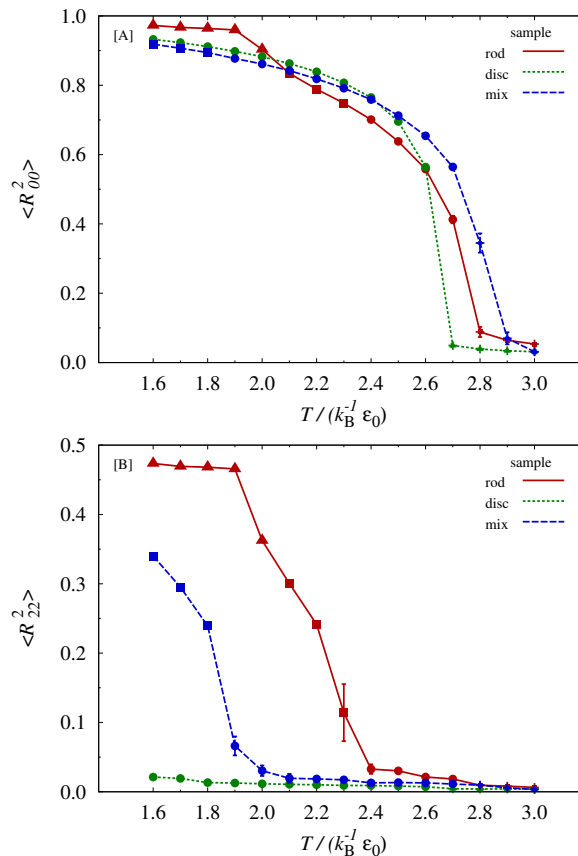


**Fig. 3** The average overall  $\langle R_{00}^2 \rangle$  (plate A), and  $\langle R_{22}^2 \rangle$  (plate B) orientational order parameters, as a function of dimensionless temperature from a cooling–down sequence of MD simulations of the  $N = 4096$  systems. See Figure 2 for additional details

The sample was maintained at constant temperature  $T^* = T/(k_B^{-1} \epsilon_0)$ , and pressure  $P^* = P/(\sigma_0^{-3} \epsilon_0) = 8$  by means of the weak coupling thermostat and barostat due to Berendsen<sup>55</sup>, with dimensionless time constants  $\tau_T = 10$ , and  $\tau_P = 100$ . Every series of MD simulations consisted of a temperature scan performed as a gradual cooling–down sequence of a well equilibrated isotropic sample. Successive runs were started from the final equilibrated configuration of the previous temperature. In all cases, equilibration runs were not shorter than 200 k time step, after which the thermodynamic observables have been sampled every 20 k time step from production runs 250 k time step long. A blocking algorithm<sup>56</sup> has been used to compute averages and error estimates. We have found isotropic (I), uniaxial nematic (N), biaxial nematic ( $N_b$ ), and biaxial smectic ( $S_b$ ) phases, but not columnar ones<sup>57</sup>.

The average uniaxial and biaxial order parameters rel-

evant to the experiment can be defined as ensemble averages with respect to the single particle distribution functions of symmetrised Wigner matrices, *i.e.* scalar products involving the particle molecular axes and the director frame axes  $\mathbf{n}$ ,  $\mathbf{m}$ , and  $\mathbf{l} = \mathbf{m} \times \mathbf{n}$ <sup>58,59</sup>

$$\langle R_{00}^2 \rangle = \left\langle \frac{3}{2} (\mathbf{z} \cdot \mathbf{n})^2 - \frac{1}{2} \right\rangle, \quad (8)$$

$$\langle R_{22}^2 \rangle = \left\langle \frac{1}{4} [(\mathbf{x} \cdot \mathbf{l})^2 - (\mathbf{x} \cdot \mathbf{m})^2 - (\mathbf{y} \cdot \mathbf{l})^2 + (\mathbf{y} \cdot \mathbf{m})^2] \right\rangle. \quad (9)$$

The order parameters are computed from the eigenvalues of single-species ordering matrices<sup>47,58</sup>, and for the one-component systems the standard algorithm<sup>58</sup> is generally sufficient. These definitions can be extended to uniform uniform multi-species mixtures, and in the Appendix we describe the simplified protocol for the present case of biaxial ellipsoids.

## 4 Results and discussion

The location of the spontaneous ordering transitions in the two single-component systems and in the mixture were determined from the average values of potential energy, orientational order parameters, and radial pair correlation functions obtained from the MD temperature scans which we now discuss in turn (the thermodynamic and ordering properties for the three families of samples are given in Tables 1, 2, and 3). No detailed free energy studies have been performed since we are interested in qualitative and semi-quantitative explorations to determine the outcome of the chosen parameterisation.

In Figure 2–A we plot the average values for the dimensionless potential energy per particle  $\langle U^* \rangle = \langle U \rangle / \epsilon_0$ . We see that there are no strong discontinuities of the energy across the phase transitions (shown in Figure 2–B as different symbols for every simulated state point). In particular, the spontaneous I–N ordering transitions for the single-component elongated and squashed systems take place with very small jumps in the average energy. This is also true for number density  $\langle \rho^* \rangle = \langle \rho \rangle / \sigma_0^{-3} = \langle 1/V \rangle N / \sigma_0^{-3}$  (given in Tables 1, 2, and 3). A similar behaviour was also observed in correspondence of the N–N<sub>b</sub> transition for the prolate particles. Only across the N<sub>b</sub>–S<sub>b</sub> (single-component elongated) and the I–N (equimolar mixture) we have found a significant discontinuity in energy and density. The  $\langle U^* \rangle$  values for the single-component disc and equimolar mixture systems are fairly close along the entire temperature range, while for the rod-like samples this was found only for

the low-temperature biaxial smectic phase. Figure 2–B summarises the sequences of phases and transition temperatures observed for the three thermotropic systems.

The order parameter profiles in Figure 3 are the most telling observables for the identification of the present temperature-driven phase transitions. Upon cooling the isotropic sample of the rod-like particles a sequence of N, N<sub>b</sub>, and S<sub>b</sub> phases are encountered (Table 1), with appreciable discontinuities in  $\langle R_{00}^2 \rangle$  only across the I–N transition. We notice that the single-component system of rod-like particles has a phase diagram similar to the one for ellipsoids with same shape but stronger lateral interactions<sup>47</sup>: all ordering transitions are shifted to lower temperatures, while the stability ranges for the N, and N<sub>b</sub> become wider.

The single-component discotic system has an I–N transition at slightly lower temperature with respect to the fluid of elongated particles, and the biaxial order parameter  $\langle R_{22}^2 \rangle$  remains zero over the entire temperature range explored by our MD simulations (Table 2). The discotic nematic phase is very stable and extends even to the lower bound of the explored temperature range, where the calamitic system is smectic. This behaviour is unusual as few mesogens forming a nematic discotic but not a columnar one are experimentally known<sup>60–63</sup>, and even with computer simulations a certain parameterisation of the anisotropic potential is necessary to observe this<sup>57,64</sup>.

The visual inspection of the equilibrated MD configurations shows that the equimolar binary mixture remains in a uniform state at all temperatures and undergoes an I–N transition at a temperature which is intermediate between those observed for the single-component fluids (Table 3). Also the uniaxial nematic phase has an order parameter  $\langle R_{00}^2 \rangle$  slightly smaller than those for the rod and disc systems. At temperatures lower than  $T^* = 1.9$  the average  $\langle R_{22}^2 \rangle$  order parameter becomes not zero and the equimolar nematic mixture becomes biaxial. We have not observed smectic phases in the explored temperature range.

The structural changes taking place in the nematic phase upon mixing have been assessed by computing the radial pair correlation function which is defined as

$$g_0(r) = \langle \delta(r - r_{12}) \rangle_{12} / (4\pi^2 \rho), \quad (10)$$

where the angular brackets  $\langle \dots \rangle_{12}$  stand for an ensemble average. Here, we concentrate on the results at  $T^* = 1.8$  where the three systems have similar  $\langle R_{00}^2 \rangle$  but quite different  $\langle R_{22}^2 \rangle$  order parameters. We see from the plot of Figure 4 that the disc–disc pairs have qualitatively similar radial pair correlation functions both in the single-component and the equimolar mixture systems

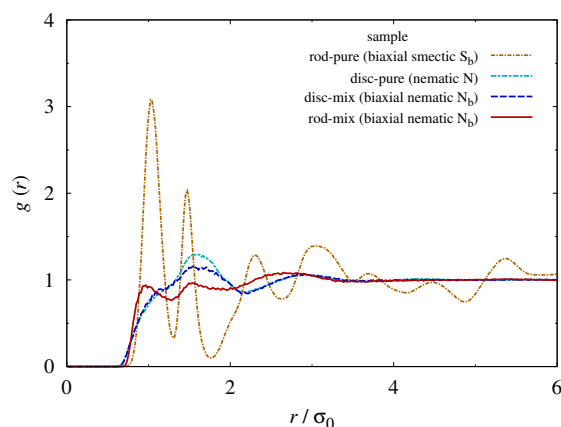


**Fig. 4** Radial correlation functions for the rod–rod and disc–disc pairs in the two single–component and the equimolar mixture samples at dimensionless temperature  $T^* = 1.8$

(even though one is a uniaxial while the other is a biaxial nematic). The same is not true for the elongated rod–rod pairs which have a typical highly ordered smectic–like radial pair correlation function in the single–component system, but one quite similar to the disc–like particles in the equimolar mixture. This result shows that even from the structural point of view the duality arising from the interaction biaxiality of the rod–like particles takes over the shape biaxiality in this mixed system.

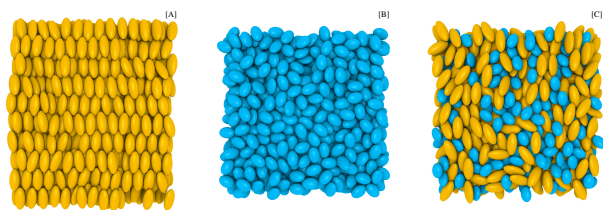


**Fig. 5** Snapshots of three systems of biaxial GB ellipsoids at dimensionless temperature  $T^* = 1.8$ : (plate A) lateral view, along the  $\mathbf{m}$  director, of the single–component  $S_b$  system formed by the rod–like particles; (plate B) top view, along the  $\mathbf{n}$  director, of the single–component  $N$  system formed by the disc–like particles; and (plate C) top view, along the  $\mathbf{n}$  director, of the single–component  $N$  system formed by the disc–like particles

To summarise, the typical features of the low temperature organisations of the three families of samples can be caught from the snapshots of Figure 5. At  $T^* = 1.8$  the single–component rod–like sample gives rise to an orthogonal biaxial smectic phase, similarly to what has been observed for the ellipsoids with same shape but stronger interactions of ref. <sup>47</sup> (even though at higher temperatures).

The single–component disc–like samples remain instead in a uniaxial discotic nematic organisation even at very low temperatures and high  $\langle R_{00}^2 \rangle$  order parameter (Figure 5–B), and do not form any columnar phase<sup>57</sup>. The equimolar mixture does not phase–separate and forms a  $N_b$  at the lowest temperatures.

There is an interesting change of mesogenic behaviour in the rod–like ellipsoids in the mixture. While in the single–component states the rods align preferentially with respect to their long axis (Figure 5–A), in the rod–disc mixture it is the short axis which has the strongest tendency to align and provides the highest degree of orientational ordering (Figure 5–C). In this respect, the elongated ellipsoids (because of their dual nature arising from the biaxiality of attractions) behave as squashed ones in the equimolar mixture. This is not what happens in the single–component system where it is the shape biaxiality which mostly determines the kind of molecular alignment, and the attractive potential only disfavours layered organisations.

As suggested by Chandrasekhar<sup>65,66</sup> one pathway towards biaxial nematics (either one– or multi–components) involves “... *preparing a mesogen that combines the features of the rod and the disc*”. However, specific design hints for building up dual behaviour were, and still are, not obvious to come by. Our computer simulations show how duality can be practically attained in several ways: matching molecular dimensions; duality in interaction via competing contributions giving *side-by-side* interactions stronger than *face-to-face*; and heterogeneous attractions comparable to homogeneous ones.

The suggestion about weakening *face-to-face* interactions may be the most difficult to come by. It could be realised with electrostatic repulsions between charges of the same sign<sup>67</sup> to counterbalance the attractive polarisation interactions which are usually stronger when two broad shaped molecules stack *face-to-face*. The enhanced heterogeneous attractions and the negative interaction biaxialities might be achieved with specific weak interactions, like hydrogen bonding between complementary lateral groups<sup>33,34</sup>.

There is a last mechanism which may be useful for the experimental realisation of  $N_b$  systems: duality in shape may be sustained by a certain degree of conformational flexibility<sup>68–70</sup> and/or shape polydispersity<sup>20,42</sup> (which are not accounted for in our simple rigid model). For instance, the mesogenic behaviour of the very flexible silicon tetrapodes of Mehl and co–workers<sup>10</sup> may arise from a rod–disc shape interconversion process<sup>68–70</sup>, providing a distribution of effective shapes resembling that of a polydispersed sample.

## 5 Conclusions

We have shown by MD computer simulations of attractive–repulsive biaxial ellipsoids that the transition temperature of  $N_b$  organisations can be lowered by mixing a biaxial nematic with a discotic one. The  $N-N_b$  transition temperature is  $\approx 20\%$  lower than that of the pure calamitic mesogen. The suppression of layered and/or stacked structures, and the miscibility over a wide temperature range encompassing isotropic and nematic phases is obtained by designing rod– and disc–like particles with a dual calamitic–discotic nature.

In view of suggesting practical guidelines to synthetic chemists we believe the most challenging design effort might be the synthesis of a disc–like mesogen with very broad and low–temperature discotic nematic range. However, the specific mesogenic dual nature of these elongated and squashed mesogens may be obtained with peripheral groups giving both weak anisotropic interactions between the sides (especially but not exclusively for the heterogeneous rod–disc pairs), and at the same time dis-favouring the *face-to-face* stacking by means of electrostatic repulsions between opposite charges on the disc plane.

The possibility of obtaining biaxial nematic mixtures at room temperature and with a wide stability range might be useful in view of technological applications of these materials towards fast–switching molecular devices. To this end, tuning the mesogenic behaviour of already known compounds by chemical modification to match the properties required to stabilise a low–temperature biaxial nematic mixture may be relatively easier than devising new classes of weakly–associating complementary molecules.

## Acknowledgements

We thank EU–STREP “*Biaxial Nematic Devices*” (BIND) FP7–216025 for financial support.

## Appendix

The computation of sample–wide (global) orientational order parameters in a multi–component sample can be performed by extending the standard single–specie protocol based on ordering matrices<sup>47,58</sup> and considering all possible outcomes based on the symmetry of the various species, and the mutual orientations of the single–constituent molecules ordering frames. However, taking into account all these cases is quite involved, so we describe here a simplified algorithm suited for mixtures of biaxial ellipsoids, postponing a more detailed discussion

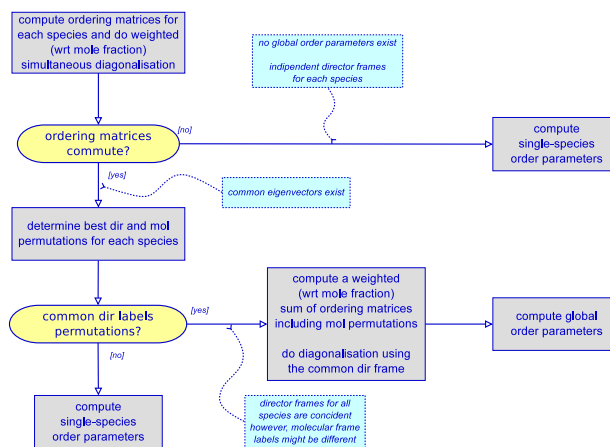


**Fig. A–1** Flowchart of the simplified algorithm used to compute global order parameters for a uniform multi–component sample of biaxial particles

to a paper specially devoted to it. This procedure relies on the assumption of the sample being a uniform monodomain (which for all our samples was checked by visual inspection). However, it can readily be extended to the computation of local order parameters in a large and possibly non–uniform system (*e.g.* due to phase separation, or the formation of local clusters, or a non–uniform director field) once a decomposition into a set of regions is available for the local mapping of single–species number densities.

The algorithm proposed for evaluating global order parameters in a MD, or Monte Carlo, configuration of biaxial ellipsoids (see the flowchart A–1) consists of a two–step procedure. To begin with, the single–species  $x$ ,  $y$ , and  $z$  ordering matrices  $\mathbf{O}_{n,\alpha} = (1/N_\alpha) \sum_i \mathbf{n}_{i,\alpha} \otimes \mathbf{n}_{i,\alpha}$  are calculated for each molecular axis (*i.e.* every  $\mathbf{n} = \mathbf{x}$ ,  $\mathbf{y}$ , and  $\mathbf{z}$  axes  $\mathbf{n}_{i,\alpha}$  for the  $i = 1, \dots, N_\alpha$  particles of species  $\alpha$ ). The total number of such ordering matrices  $\mathbf{O}_{n,\alpha}$  is  $3N_s$ , where  $N_s$  is the number of species. Then these matrices are simultaneously diagonalised and the existence of a common eigenvector frame is probed. Next, if this test was successful the second step involves the computation of three global ordering matrices, followed by their simultaneous diagonalisation, and eventually the estimation of global order parameters. This latter approach is equivalent to that of determining the principal axes of a suitable anisotropic macroscopic observable (*e.g.* the refractive index) for the whole sample. If the overall director field is truly biaxial all these  $3N_s$  ordering matrices do commute and share the same eigenvectors. However, either because the species have different local director frames, or simply because the symmetries of the orientational distributions of molecular axes are not exactly  $D_{2h}$  (*e.g.* due

to fluctuations, or the formation of local cybotactic clusters<sup>71</sup>) the ordering matrices  $\mathbf{O}_{n,\alpha}$  may not exactly commute (notice that this can also occur in a single-species system). In the former case global order parameters as such are meaningless, while the latter case still allows to define them provided the ordering matrices nearly commute, *i.e.* if an orthogonal transformation to nearly diagonal form<sup>72,73</sup> for all  $\mathbf{O}_{n,\alpha}$  exists. In particular, this is accomplished as a weighted simultaneous diagonalisation where the ordering matrices for each species concur to the global eigenvectors proportionally to the corresponding mole fraction. A convergence criterion based on the root mean square off-diagonal elements of the nearly diagonal matrices provides a suitable threshold (here we used a value of 0.05) for testing this. The orthogonal transformation to nearly diagonal form identifies three candidate global eigenvectors. However, before using them as director frame axes these eigenvectors have to be properly labelled, since for each permutation of the mutually orthogonal  $\mathbf{n}$ ,  $\mathbf{m}$ , and  $\mathbf{l}$  axes a different set of single-species order parameters can be computed (a rotation of the director frame allows the transformation from one set to the other). This is also true for the permutations of the molecular axes labels since the directions of preferential alignment can change upon transition from one phase to another (*e.g.* as we have seen here for the elongated biaxial ellipsoids). In this context, proper stands for the permutation which provides the most physically meaningful  $\langle R_{mn}^2 \rangle$  set for each specie<sup>58</sup>. For instance, the (wrong) assignment of swapped  $\mathbf{m}$ , and  $\mathbf{n}$  axes results in deceptively high  $\langle R_{22}^2 \rangle$  and rather small  $\langle R_{00}^2 \rangle$ . In practice, a convenient criterion is that of selecting the permutations giving the highest values of  $\langle R_{00}^2 \rangle$ , and the smallest positive values of  $\langle R_{22}^2 \rangle$ . The first part of this prescription is consistent with the standard algorithm for the computation of order parameters<sup>59</sup>, while the second part prevents a biased overestimation of phase biaxiality. Several strategies may be adopted at this stage. The simplest one when studying mixtures of biaxial particles consists in checking if a common permutation exists, *i.e.* all  $\mathbf{z}$  molecular axes are aligned along the same eigenvector (and, for biaxial organisations, also for the  $\mathbf{x}$  and  $\mathbf{y}$  axes), then it is possible to compute three global ordering matrices where, again, the contribution for each species is weighted according to the corresponding mole fraction. Finally, these three matrices can simultaneously be brought to nearly diagonal form, and a set of global order parameters can be defined (and computed from the eigenvalues as usual). If a common label permutation does not exist, *i.e.* the  $\mathbf{x}$ ,  $\mathbf{y}$ , and  $\mathbf{z}$  molecular axes for each species are on average aligned with respect to different permutations of the eigenvectors (*e.g.* as expected for

a biaxial mixture of uniaxial rods and discs, as is the case in ref.<sup>41</sup>), it is possible to estimate a set of global order parameters choosing as principal director  $\mathbf{n}$  the eigenvector corresponding to the highest single-species  $\langle R_{00}^2 \rangle$ , and then select the transversal directors  $\mathbf{m}$ , and  $\mathbf{l}$  to achieve the lowest biaxiality state (notice that for simplicity this has not been represented in the flowchart A-1).

## References

- 1 C. Tschierske and D. J. Photinos, *J. Mater. Chem.*, 2010, **20**, 4263–4294.
- 2 L. J. Yu and A. Saupe, *Phys. Rev. Lett.*, 1980, **45**, 1000–1003.
- 3 L. Q. Amaral, *Liq. Cryst.*, 2010, **37**, 627–640.
- 4 F. Hessel and H. Finkelmann, *Polymer Bulletin*, 1986, **15**, 349–352.
- 5 E. van den Pol, A. V. Petukhov, D. M. E. Thies-Weesie, D. V. Byelov and G. J. Vroege, *Phys. Rev. Lett.*, 2009, **103**, 258301.1–4.
- 6 E. van den Pol, D. M. E. Thies-Weesie, A. V. Petukhov, D. V. Byelov and G. J. Vroege, *Liq. Cryst.*, 2010, **37**, 641–651.
- 7 B. R. Acharya, A. Primak and S. Kumar, *Phys. Rev. Lett.*, 2004, **92**, 145506.1–4.
- 8 L. A. Madsen, T. J. Dingemans, M. Nakata and E. T. Samulski, *Phys. Rev. Lett.*, 2004, **92**, 145505.1–4.
- 9 M. Lehmann, S. Kang, C. Köhn, S. Haseloh, U. Kolb, D. Schollmeyer, Q. Wang and S. Kumar, *J. Mater. Chem.*, 2006, **16**, 4326–4334.
- 10 K. Merkel, A. Kocot, J. K. Vij, R. Korlacki, G. H. Mehl and T. Meyer, *Phys. Rev. Lett.*, 2004, **93**, 237801.1–4.
- 11 C. Cruz, J. L. Figueirinhas, D. Filip, G. Feio, A. C. Ribeiro, Y. Frère, T. Meyer and G. H. Mehl, *Phys. Rev. E*, 2008, **78**, 051702.1–16.
- 12 J. W. Goodby, *Chem. Soc. Rev.*, 2007, **36**, 1855–1856.
- 13 D. W. Bruce, *The Chemical Record*, 2004, **4**, 10–22.
- 14 T. Hegmann, J. Kain, S. Diele, G. Pelzl and C. Tschierske, *Angew. Chem. Int. Ed.*, 2001, **40**, 887–890.
- 15 R. Alben, *J. Chem. Phys.*, 1973, **59**, 4299–4304.
- 16 A. Stroobants and H. N. W. Lekkerkerker, *J. Phys. Chem.*, 1984, **88**, 3669–3674.
- 17 M. E. Neubert, *Liquid Crystals: Experimental Study of Physical Properties and Phase Transitions*, Cambridge University Press, 1st edn, 2011, ch. 2.
- 18 P. G. de Gennes and J. Prost, *The Physics of Liquid Crystals*, Oxford University Press, USA, 2nd edn, 1995.
- 19 N. V. M. R. Pratibha, *Mol. Cryst. Liq. Cryst. Letters*, 1985, **1**, 111–116.
- 20 F. M. van der Kooij and H. N. W. Lekkerkerker, *Phys. Rev. Lett.*, 2000, **84**, 781–784.
- 21 F. M. van der Kooij and H. N. W. Lekkerkerker, *Langmuir*, 2000, **16**, 10144–10149.
- 22 P. Palfy-Muhoray, J. R. de Bruyn and D. A. Dunmur, *J. Chem. Phys.*, 1985, **82**, 5294–5295.
- 23 A. G. Vanakaras and D. J. Photinos, *Mol. Cryst. Liq. Cryst.*, 1997, **299**, 65–71.
- 24 A. G. Vanakaras, A. F. Terzis and D. J. Photinos, *Mol. Cryst. Liq. Cryst.*, 2001, **362**, 67–78.
- 25 A. Chrzanowska, *Phys. Rev. E*, 1998, **58**, 3229–3236.
- 26 S. Varga, A. Galindo and G. Jackson, *J. Chem. Phys.*, 2002, **117**, 10412–10424.

- 27 S. Varga, K. Purdy, A. Galindo, S. Fraden and G. Jackson, *Phys. Rev. E*, 2005, **72**, 051704.1–19.
- 28 S. D. Peroukides, A. G. Vanakaras and D. J. Photinos, *J. Mater. Chem.*, 2010, **20**, 10495–10502.
- 29 E. do Carmo, D. B. Liarte and S. R. Salinas, *Phys. Rev. E*, 2010, **81**, 062701.1–4.
- 30 A. Galindo, A. J. Haslam, S. Varga, G. Jackson, A. G. Vanakaras, D. J. Photinos and D. A. Dunmur, *J. Chem. Phys.*, 2003, **119**, 5216–5225.
- 31 A. G. Vanakaras, S. C. McGrother, G. Jackson and D. J. Photinos, *Mol. Cryst. Liq. Cryst.*, 1998, **323**, 199–209.
- 32 J. J. Hunt, R. W. Date, B. A. Timimi, G. R. Luckhurst and D. W. Bruce, *J. Am. Chem. Soc.*, 2001, **123**, 10115–10116.
- 33 V. Cîrcu, T. J. K. Gibbs, L. Omnès, P. N. Horton, M. B. Hursthouse and D. W. Bruce, *J. Mater. Chem.*, 2006, **16**, 4316–4325.
- 34 K. Kishikawa, S. Aikyo, S. Akiyama, T. Inoue, M. Takahashi, S. Yagai, H. Aonuma and S. Kohmoto, *Soft Matter*, 2011, **7**, 5176–5187.
- 35 R. W. Date and D. W. Bruce, *J. Am. Chem. Soc.*, 2003, **125**, 9012–9013.
- 36 P. H. J. Kouwer and G. H. Mehl, *J. Mater. Chem.*, 2009, **19**, 1564–1575.
- 37 K. Jeong, A. J. Jing, B. Mansdorf, M. J. Graham, D. Yang, F. W. Harris and S. Z. D. Cheng, *Chem. Mater.*, 2007, **19**, 2921–2923.
- 38 P. H. J. Kouwer and G. H. Mehl, *J. Am. Chem. Soc.*, 2003, **125**, 11172–11173.
- 39 D. Apreutesei and G. H. Mehl, *Chem. Comm.*, 2006, 609–611.
- 40 A. G. Vanakaras, M. A. Bates and D. J. Photinos, *Phys. Chem. Chem. Phys.*, 2003, **5**, 3700–3706.
- 41 A. Cuetos, A. Galindo and G. Jackson, *Phys. Rev. Lett.*, 2008, **101**, 237802.1–4.
- 42 Y. Martínez-Ratón and J. A. Cuesta, *Phys. Rev. Lett.*, 2002, **89**, 185701.1–4.
- 43 J. G. Gay and B. J. Berne, *J. Chem. Phys.*, 1981, **74**, 3316–3319.
- 44 R. Berardi, C. Fava and C. Zannoni, *Chem. Phys. Lett.*, 1995, **236**, 462–468.
- 45 R. Berardi, C. Fava and C. Zannoni, *Chem. Phys. Lett.*, 1998, **297**, 8–14.
- 46 R. Everaers and M. R. Ejtehadi, *Phys. Rev. E*, 2003, **67**, 041710.1–8.
- 47 R. Berardi and C. Zannoni, *J. Chem. Phys.*, 2000, **113**, 5971–5979.
- 48 S. L. Altmann, *Rotations, Quaternions, and Double Groups*, Dover, New York, 2005.
- 49 R. Berardi, L. Muccioli and C. Zannoni, *J. Chem. Phys.*, 2008, **128**, 024905.1–12.
- 50 M. P. Allen and G. Germano, *Mol. Phys.*, 2006, **104**, 3225–3235.
- 51 M. P. Allen and D. J. Tildesley, *Computer Simulation of Liquids*, Oxford University Press, Oxford, 1989.
- 52 D. Frenkel and B. Smit, *Understanding Molecular Simulations, 2nd edition*, Academic Press, San Diego, 2001.
- 53 N. Matubayasi and N. M., *J. Chem. Phys.*, 1999, **110**, 3291–3301.
- 54 H. Kamberaj, R. J. Low and M. P. Neal, *J. Chem. Phys.*, 2005, **122**, 224114.1–30.
- 55 H. J. C. Berendsen, J. P. M. Postma, W. F. van Gunsteren, A. Di Nola and J. R. Haak, *J. Chem. Phys.*, 1984, **81**, 3684–3690.
- 56 H. Flyvbjerg and H. G. Petersen, *J. Chem. Phys.*, 1989, **91**, 461–466.
- 57 R. Berardi and C. Zannoni, *Mol. Cryst. Liq. Cryst.*, 2003, **396**, 177–186.
- 58 F. Biscarini, C. Chiccoli, P. Pasini, F. Semeria and C. Zannoni, *Phys. Rev. Lett.*, 1995, **75**, 1803–1806.
- 59 C. Zannoni, *The Molecular Physics of Liquid Crystals*, Academic Press, London, 1979, pp. 51–83.
- 60 S. Kumar and S. K. Varshney, *Org. Lett.*, 2002, **4**, 157–159.
- 61 S. Kohmoto, E. Mori and K. Kishikawa, *J. Am. Chem. Soc.*, 2007, **129**, 13364–13365.
- 62 S. Kumar, *Chem. Soc. Rev.*, 2006, **35**, 83–109.
- 63 H. K. Bisoyi and S. Kumar, *Chem. Soc. Rev.*, 2010, **39**, 264–285.
- 64 B. Martínez-Haya and A. Cuetos, *Phys. Rev. E*, 2010, **81**, 020701.1–4.
- 65 S. Chandrasekhar, *Mol. Cryst. Liq. Cryst.*, 1985, **124**, 1–20.
- 66 S. Chandrasekhar, *Liquid Crystals*, Cambridge University Press, 2nd edn, 1993.
- 67 S. Orlandi, L. Muccioli, M. Ricci, R. Berardi and C. Zannoni, *Chemistry Central*, 2007, **1**, 15.1–13.
- 68 P. Tolédano and A. M. F. Neto, *Phys. Rev. Lett.*, 1994, **73**, 2216–2219.
- 69 L. Longa, G. Pająk and T. Wydro, *Phys. Rev. E*, 2007, **76**, 011703.1–6.
- 70 P. K. Karahaliou, A. G. Vanakaras and D. J. Photinos, *J. Chem. Phys.*, 2009, **131**, 124516.1–14.
- 71 A. G. Vanakaras and D. J. Photinos, *J. Chem. Phys.*, 2008, **128**, 154512.1–6.
- 72 B. N. Flury and G. Constantine, *Applied Statistics*, 1985, **34**, 177–183.
- 73 B. N. Flury and W. Gautschi, *SIAM J. Sci. Stat. Comput.*, 1986, **7**, 169–184.

**Table 1** Average orientational order parameters  $\langle R_{00}^2 \rangle$ , and  $\langle R_{22}^2 \rangle$ , dimensionless potential energy per particle  $\langle U^* \rangle$ , and number density  $\langle \rho^* \rangle$  for the MD simulations of the system  $N = 4096$  biaxial rod-like GB ellipsoids giving isotropic (I), nematic (N), biaxial nematic ( $N_b$ ), and biaxial smectic ( $S_b$ ) phases as indicated. Estimated rms errors on the block averages are also given

$T^*$	$\langle R_{00}^2 \rangle$	$\langle R_{22}^2 \rangle$	$\langle U^* \rangle$	$\langle \rho^* \rangle$	phase
1.6	$0.973 \pm 0.000$	$0.474 \pm 0.000$	$-12.763 \pm 0.004$	$0.3689 \pm 0.0001$	$S_b$
1.7	$0.967 \pm 0.000$	$0.469 \pm 0.000$	$-12.278 \pm 0.003$	$0.3646 \pm 0.0000$	$S_b$
1.8	$0.964 \pm 0.001$	$0.468 \pm 0.002$	$-11.899 \pm 0.062$	$0.3613 \pm 0.0005$	$S_b$
1.9	$0.959 \pm 0.001$	$0.466 \pm 0.001$	$-11.453 \pm 0.072$	$0.3570 \pm 0.0005$	$S_b$
2.0	$0.903 \pm 0.000$	$0.362 \pm 0.001$	$-7.927 \pm 0.005$	$0.3335 \pm 0.0000$	$S_b$
2.1	$0.834 \pm 0.001$	$0.300 \pm 0.003$	$-6.185 \pm 0.024$	$0.3222 \pm 0.0001$	$N_b$
2.2	$0.789 \pm 0.001$	$0.241 \pm 0.002$	$-5.334 \pm 0.002$	$0.3144 \pm 0.0000$	$N_b$
2.3	$0.748 \pm 0.002$	$0.114 \pm 0.041$	$-4.616 \pm 0.057$	$0.3069 \pm 0.0005$	$N_b$
2.4	$0.701 \pm 0.002$	$0.033 \pm 0.007$	$-4.079 \pm 0.015$	$0.3008 \pm 0.0001$	N
2.5	$0.638 \pm 0.004$	$0.030 \pm 0.003$	$-3.627 \pm 0.008$	$0.2952 \pm 0.0001$	N
2.6	$0.558 \pm 0.006$	$0.021 \pm 0.001$	$-3.190 \pm 0.013$	$0.2897 \pm 0.0001$	N
2.7	$0.413 \pm 0.011$	$0.019 \pm 0.002$	$-2.678 \pm 0.022$	$0.2835 \pm 0.0002$	N
2.8	$0.088 \pm 0.015$	$0.009 \pm 0.001$	$-2.105 \pm 0.011$	$0.2767 \pm 0.0001$	I
2.9	$0.064 \pm 0.003$	$0.008 \pm 0.000$	$-1.927 \pm 0.001$	$0.2733 \pm 0.0000$	I
3.0	$0.054 \pm 0.002$	$0.006 \pm 0.000$	$-1.786 \pm 0.002$	$0.2704 \pm 0.0000$	I

**Table 2** Average orientational order parameters  $\langle R_{00}^2 \rangle$ , and  $\langle R_{22}^2 \rangle$ , dimensionless potential energy per particle  $\langle U^* \rangle$ , and number density  $\langle \rho^* \rangle$  for the MD simulations of the system of  $N = 4096$  biaxial disc-like GB ellipsoids giving isotropic (I), and uniaxial nematic (N) phases as indicated. Estimated rms errors on the block averages are also given

$T^*$	$\langle R_{00}^2 \rangle$	$\langle R_{22}^2 \rangle$	$\langle U^* \rangle$	$\langle \rho^* \rangle$	phase
1.6	$0.932 \pm 0.000$	$0.021 \pm 0.002$	$-13.009 \pm 0.001$	$0.5216 \pm 0.0000$	N
1.7	$0.923 \pm 0.000$	$0.019 \pm 0.002$	$-12.391 \pm 0.008$	$0.5134 \pm 0.0001$	N
1.8	$0.911 \pm 0.000$	$0.013 \pm 0.001$	$-11.772 \pm 0.002$	$0.5051 \pm 0.0000$	N
1.9	$0.898 \pm 0.001$	$0.013 \pm 0.001$	$-11.168 \pm 0.002$	$0.4969 \pm 0.0000$	N
2.0	$0.882 \pm 0.001$	$0.011 \pm 0.000$	$-10.569 \pm 0.008$	$0.4887 \pm 0.0001$	N
2.1	$0.863 \pm 0.001$	$0.011 \pm 0.000$	$-9.966 \pm 0.008$	$0.4805 \pm 0.0001$	N
2.2	$0.839 \pm 0.000$	$0.010 \pm 0.000$	$-9.336 \pm 0.002$	$0.4720 \pm 0.0000$	N
2.3	$0.807 \pm 0.000$	$0.009 \pm 0.000$	$-8.675 \pm 0.004$	$0.4632 \pm 0.0001$	N
2.4	$0.765 \pm 0.001$	$0.009 \pm 0.000$	$-7.967 \pm 0.006$	$0.4540 \pm 0.0001$	N
2.5	$0.695 \pm 0.003$	$0.008 \pm 0.000$	$-7.117 \pm 0.009$	$0.4434 \pm 0.0001$	N
2.6	$0.564 \pm 0.007$	$0.007 \pm 0.000$	$-5.992 \pm 0.032$	$0.4303 \pm 0.0003$	N
2.7	$0.049 \pm 0.005$	$0.004 \pm 0.000$	$-4.185 \pm 0.002$	$0.4107 \pm 0.0000$	I
2.8	$0.039 \pm 0.002$	$0.004 \pm 0.000$	$-3.949 \pm 0.005$	$0.4053 \pm 0.0000$	I
2.9	$0.034 \pm 0.001$	$0.004 \pm 0.000$	$-3.754 \pm 0.004$	$0.4003 \pm 0.0000$	I
3.0	$0.031 \pm 0.001$	$0.004 \pm 0.000$	$-3.591 \pm 0.002$	$0.3957 \pm 0.0000$	I

**Table 3** Average orientational order parameters  $\langle R_{00}^2 \rangle$ , and  $\langle R_{22}^2 \rangle$ , dimensionless potential energy per particle  $\langle U^* \rangle$ , and number density  $\langle \rho^* \rangle$  for the MD simulations of the equimolar mixture of  $N = 2048$  prolate and  $N = 2048$  oblate biaxial GB ellipsoids giving isotropic (I), nematic (N), and biaxial nematic (N<sub>b</sub>) phases as indicated. Estimated rms errors on the block averages are also given

$T^*$	$\langle R_{00}^2 \rangle$	$\langle R_{22}^2 \rangle$	$\langle U^* \rangle$	$\langle \rho^* \rangle$	phase
1.6	$0.918 \pm 0.000$	$0.340 \pm 0.001$	$-12.820 \pm 0.003$	$0.4214 \pm 0.0000$	N <sub>b</sub>
1.7	$0.907 \pm 0.001$	$0.295 \pm 0.002$	$-11.938 \pm 0.005$	$0.4133 \pm 0.0000$	N <sub>b</sub>
1.8	$0.894 \pm 0.001$	$0.239 \pm 0.004$	$-11.110 \pm 0.014$	$0.4053 \pm 0.0001$	N <sub>b</sub>
1.9	$0.877 \pm 0.001$	$0.066 \pm 0.014$	$-10.203 \pm 0.011$	$0.3964 \pm 0.0001$	N
2.0	$0.861 \pm 0.001$	$0.030 \pm 0.008$	$-9.603 \pm 0.005$	$0.3898 \pm 0.0000$	N
2.1	$0.842 \pm 0.001$	$0.019 \pm 0.006$	$-9.056 \pm 0.008$	$0.3834 \pm 0.0001$	N
2.2	$0.818 \pm 0.003$	$0.019 \pm 0.002$	$-8.527 \pm 0.009$	$0.3772 \pm 0.0001$	N
2.3	$0.791 \pm 0.001$	$0.017 \pm 0.001$	$-8.006 \pm 0.008$	$0.3710 \pm 0.0001$	N
2.4	$0.759 \pm 0.001$	$0.013 \pm 0.001$	$-7.468 \pm 0.006$	$0.3647 \pm 0.0001$	N
2.5	$0.712 \pm 0.002$	$0.013 \pm 0.002$	$-6.907 \pm 0.008$	$0.3580 \pm 0.0001$	N
2.6	$0.654 \pm 0.005$	$0.013 \pm 0.001$	$-6.324 \pm 0.017$	$0.3512 \pm 0.0001$	N
2.7	$0.564 \pm 0.007$	$0.011 \pm 0.001$	$-5.667 \pm 0.015$	$0.3436 \pm 0.0001$	N
2.8	$0.345 \pm 0.028$	$0.010 \pm 0.001$	$-4.736 \pm 0.053$	$0.3337 \pm 0.0004$	I
2.9	$0.070 \pm 0.017$	$0.006 \pm 0.001$	$-4.098 \pm 0.010$	$0.3261 \pm 0.0001$	I
3.0	$0.031 \pm 0.005$	$0.003 \pm 0.000$	$-3.876 \pm 0.006$	$0.3221 \pm 0.0000$	I